2.4 A POTENTIAL VORTICITY AND WAVE ACTIVITY FLUX DIAGNOSIS OF OPTIMAL PERTURBATION EVOLUTION

Michael C. Morgan

University of Wisconsin - Madison
Madison, Wisconsin

1. INTRODUCTION

Singular vectors (SVs), or "optimal perturbations", are those perturbations which linearly amplify most rapidly for a prescribed metric (norm), over a finite time interval (τ_{opt}), for a given basic state. SVs are initially localized in space and have structures which tilt upshear. Furthermore, the initial SV perturbation is generally confined to subsynoptic scales, and, for baroclinic flows, the perturbation amplitude is maximized in the lower troposphere (*e.g.,* Mukougawa and Ikeda, 1994; Buizza and Palmer, 1995). For a given flow, it is inferred from the localization of the initial SV perturbation in the lower troposphere that the maximum sensitivity for that flow is in the lower troposphere - an inference seemingly at odds with "potential vorticity (PV) thinking" which suggests that the dynamically important regions of a flow should be found in the upper troposphere and near the earth's surface where the largest gradients of PV are typically observed (*e.g.*, Morgan and Nielsen-Gammon, 1998). Palmer *et al*. (1998) suggest that this difference is "consistent with the differences between Lagrangian advection *vs.* wave [activity] propagation." It is this distinction which this presentation addresses and clarifies.

Briefly, PV based sensitivity *estimates* focus on prominent perturbations in upper tropospheric PV and near surface potential temperature (PT) in regions in which these perturbations may amplify due to favorable advections of PV (PT) *along* isentropic surfaces (the earth's surface). On the other hand, wave activity diagnostics describe the propagation of wave activity *along or across* isentropic surfaces. Wave activity density, A, defined as:

$$A \equiv \frac{1}{2}\frac{\overline{q'^2}}{\overline{q}_y} \tag{1.1}$$

may be viewed as a local normalized measure of disturbance "waviness." Wave activity density is one-half the zonally averaged quasi-geostrophic (QG) potential enstrophy, q'^2,weighted by the inverse of the magnitude of the basic state QGPV gradient, $\overline{q}_y$ supporting the disturbance. Wave activity density satisfies a conservation relation:

$$\frac{\partial A}{\partial t} + \nabla \cdot \mathbf{F} = S, \tag{1.2}$$

where **F** is the Eliassen-Palm (E-P) flux vector, and S represents sources/sinks of wave activity density. For conservative flows, Palmer *et al.* argue that the maximum sensitivity inferred from SV analyses is consistent with conservation of wave activity density as small amplitude (as measured in terms of wave enstrophy) perturbations amplify as they propagate from regions of small PV gradient to regions of larger PV gradient. Palmer *et al.* (1998) propose that the crucial issue in reconciling these seemingly disparate views of sensitivity is whether the component of lower tropospheric PV anomalies that projects onto vertically propagating waves is large enough to create significant perturbations in the upper tropospheric PV.

In this presentation, using both PV and E-P flux diagnostics, the mechanisms by which the midtropospheric PV anomalies optimally excite the upper and lower tropospheric PV and PT waves are described, and it is demonstrated that indeed, initially small amplitude, lower to middle tropospheric PV anomalies can effectively influence the evolution of both the upper tropospheric PV and the lower tropospheric PT.

A description of the SV evolution in the Eady (1949) model for the L_2 norm of streamfunction amplitude is presented in Section 2. In Section 3, a review and application of the PV inversion and wave activity diagnostics used in describing the SV evolution is found. A brief description of SV evolution in the Green (1960) model is given in Section 4. Section 5 contains a summary and brief discussion of results.

2. DESCRIPTION OF SV EVOLUTION

For the calculations to follow, the basic state was characterized by vertical shear of 3 $ms^{-1}km^{-1}$ in a troposphere of 10 km depth, a constant Brunt-Väisälä frequency of $10^{-2}s^{-1}$, and a Coriolis parameter, $f_0 = 10^{-4}$ s^{-1}. The nondimensional time t = 1 corresponds to 27 hours. The nondimensional zonal wave number k = 1 corresponds to a wavelength of approximately 3142 km. For

* Corresponding author address: Michael C. Morgan, University of Wisconsin - Madison, Department of Atmospheric and Oceanic Sciences, 1225 W. Dayton Street, Madison, Wisconsin 53706

email: morgan@aurora.meteor.wisc.edu

this study, the meridional wave number is zero.

2.1 *SV development for k* = 1 *and* τ_{opt} = 4.2

Figs.1 a, d, g, and j show the streamfunction evolution for the τ_{opt} = 4.2 SV at the selected times t = 0, 3, 4.2, and 6. The streamfunction is initially characterized by an upshear tilt and maximum amplitude in the mid-troposphere (Fig. 1a). We note also the lack of streamfunction structure near the upper and lower boundaries - from which we may infer that the initial BTAs as well as the initial boundary meridional velocities associated with the SV are small. The streamfunction amplifies by a factor of 59.26 by optimization time, the maximum amplitude shifts to the boundaries, and the degree to which the SV streamfunction leans against the shear diminishes (Fig. 1g). By t = 6 (Fig. 1j), the disturbance has amplified by a factor of 281.89 compared with its initial amplitude. The disturbance at this time (and at the optimization time) resembles the unstable (growing) mode.

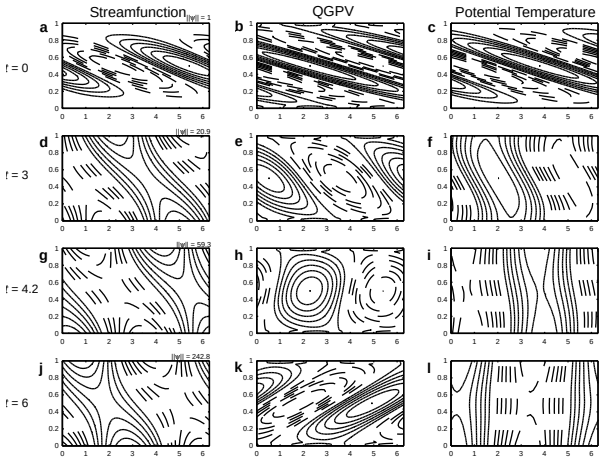

Fig. 1 Evolution of streamfunction, QGPV, and potential temperature for the k = 1, τ_{opt} = 4.2 SV.

Figs. 1 b, e, h, and k show the PV evolution for the τ_{opt} = 4.2 SV at the same selected times as for the streamfunction. The PV for this SV initially leans strongly upshear and is also concentrated in the midtroposphere (Fig. 2b). Unlike the streamfunction, however, the PV does not amplify as the disturbance evolves: there are no sources or sinks of perturbation PV. As a consequence, the tilt of the PV against the shear is diminished as the shear flow advects the SV PV. By optimization time (Fig. 1e), the PV has become more isotropic in structure and is nearly vertical. The shear continues to tilt over the PV so that by t = 6, the PV is tilted downshear (Fig. 1h).

Figs 1 c, f, i, and l show the evolution of the potential temperature perturbations associated with the τ_{opt} = 4.2 SV. For the evolution of this SV, the only dynamically important feature of the perturbation potential temperature distribution is its distribution along the upper and lower boundaries. As inferred above, at t = 0, the magnitude of the temperature perturbations is smallest along the boundaries. We note that the PT perturbation in the interior is consistent with the PV distribution - below (above) positive (negative) PV perturbations are found negative (positive) PT perturbations. The perturbation potential temperature structure has a similar upshear tilt as the PV. As the SV evolves, the maxima in the potential temperature anomalies shifts to the boundaries. At t = 4.2 (Fig. 1f), the PT perturbations still have an upshear tilt - indicating that a GNM structure has not yet emerged from the initial conditions. By t = τ_{opt} + 2 days, the thermal structure acquires a downshear tilt indicating that a GNM structure has begun to dominate the developing disturbance.

2.2 *SV development for k* = 5 *and* τ_{opt} = 1.8

The structure of the initial SV for k = 5, τ_{opt} = 1.8 looks qualitatively similar to the corresponding SV structure with k = 1, τ_{opt} = 4.2: an initially upshear tilted perturbation streamfunction and PV (Figs. 2 a and b). By t = τ_{opt} = 1.8 (Fig. 2g), the SV has developed absolute maxima in the perturbation streamfunction at the upper and lower boundaries while still possessing a relative maximum in streamfunction in the mid-troposphere. The norm of the streamfunction is 30.32. For t = 4. (Fig. 2j), the streamfunction is maximized at the boundaries, and resembles the streamfunction associated with a combination of upper and lower boundary edge waves.

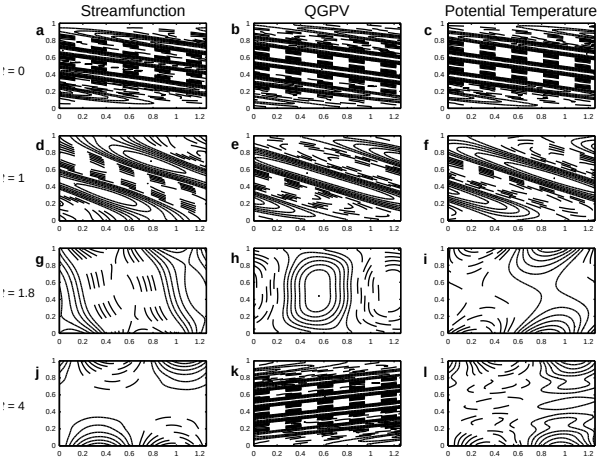

Fig. 2 As in Fig.1 except for the k = 5, τ_{opt} = 1.8 SV

For this SV, the QGPV structure and evolution (Figs. 2 b, e, h, and k) resembles that of the k = 1 SV: the PV is tilted over by the shear flow, becoming vertical at the optimization time (by construction). From then on, the PV tilts downshear.

The potential temperature perturbations associated with the k = 5, τ_{opt} = 1.8 SV are initially upshear tilted, with small BTAs (Fig. 2c). By optimization time and time intervals beyond, the potential temperature perturbations are maximized along the upper and lower boundaries (Figs. 2 i and l).

3. DIAGNOSIS OF SV EVOLUTION

The only mechanisms that lead to amplification of SV streamfunction in the Eady model are PV superposition and amplification of the SV boundary thermal anomalies (BTAs). In this section we present diagnosis of SV evolution using a PV diagnosis and a combination of PV and wave activity flux diagnoses.

3.1 *A potential vorticity diagnosis*

Using the technique of piecewise PV inversion (i.e., Davis and Emanuel, 1991) we may attribute specific

wind and temperature perturbations to specific parts of the SV PV-θ distribution. We partition the SV PV-θ distribution into the interior QGPV (SV PV) and the boundary potential temperature perturbations (SV BTA). We define:

$v_{pv}' = \dfrac{\partial \psi_{pv}}{\partial x}$: meridional velocity attributed to SV PV,

$v_{\theta}' = \dfrac{\partial \psi_{\theta}}{\partial x}$: meridional velocity attributed to SV BTA,

$\theta_{pv}' = \dfrac{\partial \psi_{pv}}{\partial z}$: PT attributed to SV PV, and

$\theta_{\theta}' = \dfrac{\partial \psi_{pv}}{\partial z}$: PT attributed to SV BTA.

Diagnosis of SV amplification from a PV perspective requires a diagnosis of both the amplification of the SV BTAs and the superposition of the interior SV PV anomalies. Diagnosis of the amplification of the BTAs may be inferred by considering the amplification of the meridional wind attributed to either the upper or lower BTAs. For this purpose, we diagnose the amplification of the upper BTA by examining the amplification of the meridional wind (v_T) attributed to the upper (top) BTA. Likewise, superposition of interior PV may be diagnosed by examining the amplification of the meridional wind attributed to the interior PV anomaly (v_{PV}) - this wind should be a maximum at the time of maximum superposition. For brevity, a set of diagnostics for the k = 1 SV are presented.

Fig. 3a shows the evolution of the magnitudes of the lower boundary meridional velocities attributed to the interior PV (v_{PV}), the upper BTA (v_T), and the sum of both velocities (v_{PV}+ v_T). The amplification of v_T indicates that the upper BTA is also amplifying. Furthermore, evidence for the superposition of the interior PV is observed as v_{PV}

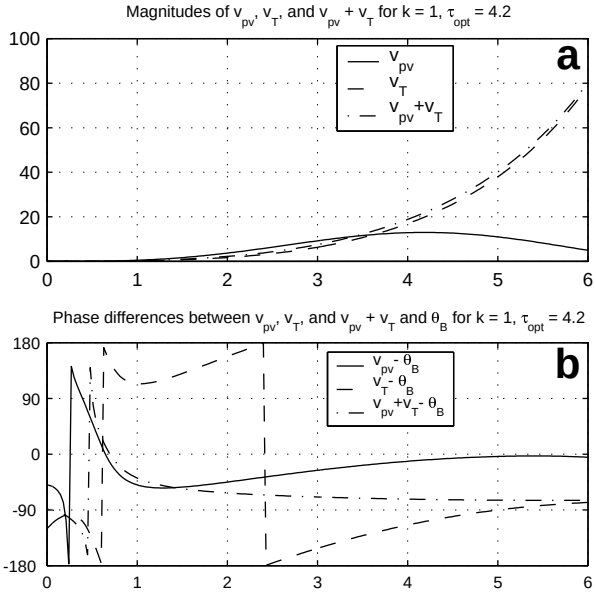

Fig. 3 (a) Magnitudes of v_T, v_{PV}, and v_T +v_{PV}; (b) phase differences between v_T, v_{PV}, and v_T +v_{PV} and θ_B.

is maximized at the same time the PV is (t = 4.2)Note also that until time t = 3.6, the largest magnitude of the two advecting velocities is v_{PV}. Following that time, the magnitude of v_T exceeds that of v_{PV}.

The amplification of the lower BTAs (θ_B) is the result of the advections of lower boundary potential temperature by winds attributed to the upper boundary temperature anomaly and winds attributed to the interior PV anomalies. The evolution of the phase differences between v_{PV} and θ_B and v_T and θ_B is shown in Fig. 3b. With the exception of the short time intervals early in the SV development, the phase difference, ϕ, between v_{PV} and θ_B is within $\pm 90^\circ$ for all times, with ϕ decreasing to nearly 0^0 by t = 4.2. On the other hand, the phase relationship between v_T and θ_B is unfavorable until approximately beyond t = 5. That the phase difference between v_T and θ_B is not within $\pm 90^\circ$ until after t = 5 indicates that NM growth does not begin until after that time. This is consistent with the upshear (downshear) tilted thermal structure seen at t = 4.2 (t = 6.0) in Fig. 1i (Fig. 1l).

3.2 *A partitioned wave activity flux diagnosis*

For the Eady model, the E-P flux vector **F**:

$$\mathbf{F} = (-\overline{u'v'}, \frac{\overline{v'\theta'}}{S}), \qquad (3.1)$$

has only a vertical component. Because the vertical shear of the zonal wind is taken to be positive in the Eady model, it may be shown that growing disturbances (i.e., those disturbances with increasing energy) are characterized by an upward directed E-P flux vector.

By combining the PV diagnostic tools presented above with diagnosis of changes in the flux of wave activity diagnosis, we may better apprehend the relative importance of various development mechanisms as well as the relationships between the diagnostics. In addition to a PV partitioning of the streamfunction field, we may also partition the vertical component of the SV EP-flux into "interaction terms":

$$\overline{v'\theta'} = \overline{v_{pv}'\theta_{pv}'} + \overline{v_{pv}'\theta_{\theta}'} + \overline{v_{\theta}'\theta_{pv}'} + \overline{v_{\theta}'\theta_{\theta}'}. \qquad (3.2)$$

We denote the four interaction terms on the right hand side of (3.2) as PV-PV, PV-B, B-PV, and B-B respectively. As an example, the term PV-B represents the meridional heat flux of thermal anomalies attributed to the BTAs by the meridional wind attributed to the PV anomalies (i.e., $\overline{v_{pv}'\theta_{\theta}'}$).

The PV-PV term may be used to diagnose the PV superposition mechanism. The PV-B term is associated with horizontal advection of PT by winds attributed to interior PV anomalies. This term will be largest nearest the boundaries where horizontal advections of potential temperature are not canceled by vertical motions. The B-PV term diagnoses the interactions of the BTAs with interior PV anomalies. Mutual interactions between the BTAs on opposing boundaries are diagnosed with the B-B term. This term will be characterized by its vertical uniformity (i.e., the flux it represents will be non-divergent) in the interior of the domain. For growing long-wave disturbances, the flux will increase for all time, while for short wave disturbances, the flux will alternate between (positive) upward and downward (negative).

3.2.1 *Diagnosis for the k = 1 SV*

Vertical-time sections of the E-P flux are shown in

Fig. 4a for the k = 1, τ_{opt} = 4.2 SV. $\overline{v'\theta'}$ associated with the developing SVs is initially negative nearest the upper and lower boundaries and maximized in the interior. Following t = 0.6, $\overline{v'\theta'}$ is positive and slowly increases until approximately t = 5.0. Thereafter, $\overline{v'\theta'}$ increases more rapidly. While the vertical component of the E-P flux is maximized at the boundaries, the E-P fluxes are nearly constant with height in the interior.

The time evolution of the terms which compose the vertical component of the E-P flux as partitioned in (3.2): PV-PV, PV-B, B-PV, and B-B, are shown in Figs. 4 b-e respectively. The PV-PV term (Fig. 4b), which represents the mechanism of PV superposition, begins to increase in the mid-troposphere, reaching a maximum at approximately t = 3, and then diminishes to zero by t = 4.1. The PV-PV term subsequently decreases - to a minimum at t = 5.3, before increasing once again. This vertical-time distribution of the PV-PV term is consistent with the PV structure and evolution previously described in section 3a. Because the thermal anomalies and the meridional wind perturbations attributable to the interior PV anomalies are largest in the midtroposphere, $\left\|\overline{v_{pv}'\theta_{pv}'}\right\|$ is maximized in the mid-troposphere. As the PV structures are tilted from upshear to downshear, the PV-PV term first diagnoses upward wave activity propagation and then, following $t = \tau_{Orr}$, downward wave propagation.

The PV-B term which, at the boundaries, is associated with v_{PV} amplifying BTAs, is maximized at the boundaries. With the exception of the initial time, this term is always positive. At approximately t = 5.3, the PV-B term is maximized at the lower boundary. Thereafter, the PV-B term decreases. The B-PV term is minimized in the mid-troposphere and is largely negative throughout most of the domain. The minimum values in the θ-PV term are reached first at approximately t = 3, and once more at the end of the time interval shown (t = 6). The behaviors of the PV-B and B-PV terms are consistent with the phase differences between v_{PV} and θ_B and v_T and θ_B described earlier - in those time intervals for which the phase differences are $-90° < \phi < 90°$, the PV-B and B-PV terms are positive (Figs. 4c and 4d).

The B-B term, which represents the mutual interaction between the opposing BTAs indicates downward propagation of wave activity until time t = 5, and then rapidly increasing, upward wave activity propagation beyond that time (Fig. 4e). This behavior is consistent with the phase difference between v_T and θ_B described earlier. Recall (Fig. 3b) that this phase difference was unfavorable for amplification of the lower BTA until t = 5. As anticipated, the B-B term is constant with respect to height in the interior. This diagnostic indicates that while the streamfunction structure at t = 4.2 resembles that of the GNM, the downward directed E-P fluxes indicate that the GNM has yet to have emerged from the initial perturbation.

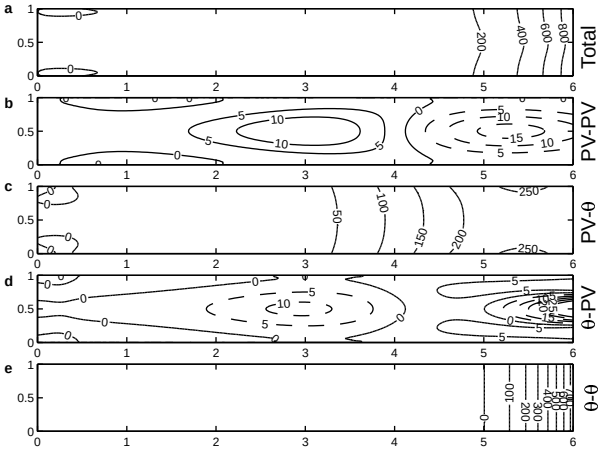

Fig. 4 For the k =1 SV, (a) total E-P flux and (b) PV-PV, (c) PV-θ, (d) θ-PV, and (e) θ–θ contributions to the E-P flux.

3.2.2 *Diagnosis for the k = 5 SV*

Fig. 5 displays the structure and evolution of the E-P flux and the PV partitioned terms which compose the flux for the k = 5, τ_{opt} = 1.8 SV. The flux, which is positive throughout most of the domain, slowly increases over the time interval $0 < t < 1.5$ (Fig. 14a). Maximum values of the flux are found in the middle of the domain. For $1.5 < t < 2$, the flux more rapidly increases along the upper and lower boundaries, and rapidly decreases in the center of the domain becoming negative for $t < 1.8$. For $t > 2$, the fluxes in the mid-troposphere reach a minimum at t = 2.25, before slowly increasing, while fluxes just inside the boundaries slowly decrease while remaining positive.

The magnitude of the PV-PV term is maximized in the mid-troposphere (Fig. 5b). It has a distribution most prominently centered around the time $t = \tau_{opt} = \tau_{Orr}$ = 1.8, the time of maximum superposition. Upward directed wave activity fluxes are maximized at t = 1.5, while downward directed fluxes are maximized at time t = 2.1. As was seen in the long wave case, the distribution of the wave activity fluxes associated with the PV-PV term are consistent with the superposition of like-signed PV anomalies.

The PV-B term is relatively small until approximately t = 1.5, when the upward E-P fluxes nearest the boundaries rapidly increase (Fig. 5c). These fluxes are maximized at t = 2 and remain positive along the boundaries until t = 3. The fluxes in the middle of the domain become negative at t = 2.25.

The B-PV term reaches a relative maximum just inside of the upper and lower boundaries at t = 1.9 (Fig.

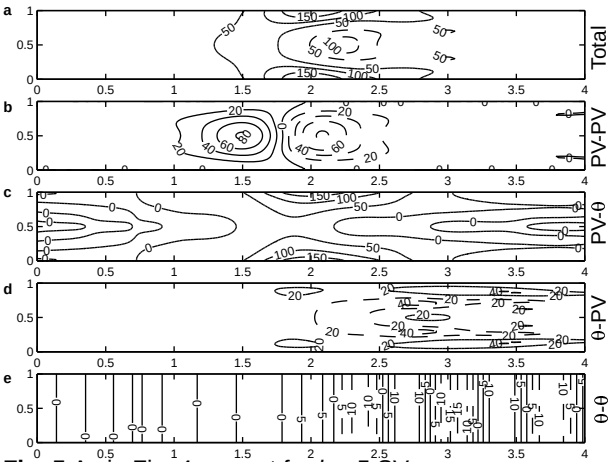

Fig. 5 As in Fig. 4, except for k = 5 SV.

5 d). In the mid-troposphere, the E-P fluxes are directed downward for $1.8 < t < 2.5$. For $t > 2.5$, the vertical distribution of the E-P fluxes is characterized by alternating upward and downward E-P fluxes.

The B-B term is characterized by a vertically uniform, alternating upward and downward directed E-P flux (Fig. 5e). The flux increases in magnitude and is distinguished by a more constant period following $t = 1.8$.

4. SV DEVELOPMENT WITH β INCLUDED

Fig. 6 (as in Figs. 1 and 2) shows the evolution of a longwave SV in the Green (1960) model. Most conspicuous is the confinement of the SVs perturbation streamfunction, QGPV, and PT to the lower troposphere. This confinement is more severe with increasing optimization time (not shown). The subsequent evolution of the SV resembles that of the Eady model $k = 1$ SV (compare Fig. 1 with Fig. 6) although there are asymmetries in the perturbation amplitudes between the upper and lower boundaries.

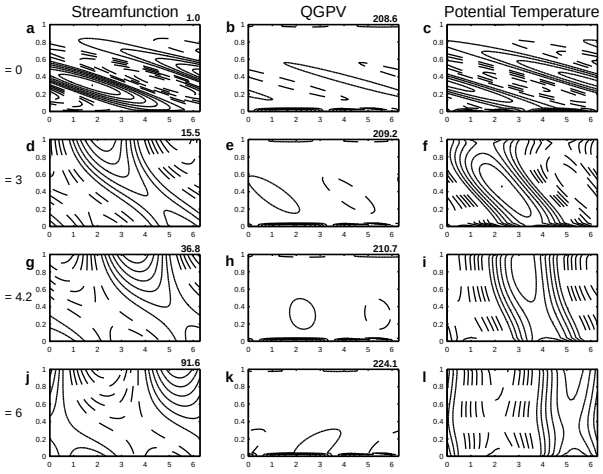

Fig. 6 As in Fig. 1, except for $k = 1$ and $\beta = 1.4 \times 10^{-11} m^{-1} s^{-1}$.

5. DISCUSSION AND SUMMARY

A diagnosis of SV evolution (computed for the L_2 streamfunction norm) in the Eady model using PV and E-P flux diagnostics is performed. In addition, a partitioning of the vertical component of the E-P flux vector based on the results of the piecewise PV inversion is introduced to more clearly elucidate the fundamental mechanisms for SV amplification.

The initial PV structures of the Eady model SVs on both the long and short wave sides of the Eady model short wave cutoff are characterized by initially upshear tilted interior PV anomalies. The results of the PV and the E-P flux diagnostics for optimal perturbations reveal a three stage process for the SV evolution: 1) A superposition of interior PV anomalies (diagnosed by a positive vertical component of the E-P flux PV-PV term), 2) a subsequent intensification (characterized by maxima in the E-P flux near the boundaries) of the SV BTAs by winds attributed to interior PV, and 3) finally a transient or sustained mutual interaction between the BTAs (associated with a nearly non-divergent interior E-P flux dominated by the B-B term).

In comparison with the Eady model, inclusion of β results in the initial Green model SV perturbation structures being confined to the lower troposphere. Attendant with this sequestering of the SV perturbations to the lower troposphere, is a reduction (increase) of the initial upper (lower) SV boundary perturbation potential temperature for SVs of large wavelength and a decrease in the meridional component of the wind along the lower boundary. The degree to which the initial SV perturbations are concentrated in the lower troposphere is governed by the length of the SV optimization interval: the longer τ_{opt}, the more confined the SV perturbations are to the lower troposphere.

The inclusion of β has a modest effect on the SV amplification; for relatively long waves, the amplification factor decreases, while for relatively short waves, the amplification factor increases. A further distinction between SVs with and without β is that the onset of modal growth is significantly delayed.

Further discussion of these results as well as a more detailed description of the methodology used may be found in Morgan (2001a,b).

Acknowledgments

This work was supported by National Science Foundation Grant ATM-9810916 and by a University of Wisconsin-Madison 1999-2001 Vilas Associates award.

6. REFERENCES

Buizza, R., and T. Palmer, 1995: The singular vector structure of the atmospheric global circulation. *J. Atmos. Sci.*, **52**, 1434 - 1456.

Davis, C. A., and K. Emanuel, 1991: Potential vorticity diagnostics of cyclogenesis. *Mon. Wea. Rev.*, **119**, 424 - 439.

Eady, E., 1949: Long waves and cyclone waves. *Tellus*, **1**, 33 - 42.

Green, J., 1960: A problem in baroclinic instability. *Quart. J. Royal Meteor. Soc.,* **86**, 237 - 251.

Morgan, M., 2001a: A potential vorticity and wave activity diagnosis of optimal perturbation evolution., *J. Atmos. Sci.*, accepted.

Morgan, M., 2001b: The effect of gradients of planetary vorticity on optimal perturbation structure and evolution., *J. Atmos. Sci.*, submitted.

Morgan, M., and J. Nielsen-Gammon, 1998: Using tropopause maps to diagnose midlatitude weather systems., *Mon. Wea. Rev.*, **126**, 2555 - 2579.

Mukougawa, H., and T. Ikeda, 1994: Optimal excitation of baroclinic waves in the Eady model. *J. Met. Soc. Japan*, **72**, 499-513.

Palmer, T., R. Gelaro, J. Barkmeijer, and R. Buizza, 1998: Singular vector, metrics, and adaptive observations. *J. Atmos. Sci.*, **55**, 633-653.